Temperatures of Anvil Clouds and Radiative Tropopause in a Wide Array of Cloud-Resolving Simulations

Seth Seidel and Da Yang

University of California, Davis

Lawrence Berkeley National Laboratory

Corresponding authors:

Seth Seidel (sdseidel@ucdavis.edu)

Da Yang (dayang@ucdavis.edu)

ABSTRACT

We present ninety-nine cloud-resolving simulations to study how temperatures of anvil clouds and radiative tropopause change with surface warming. Our simulation results show that the radiative tropopause warms at approximately the same rate as anvil clouds. This relationship persists across a variety of modeling choices, including surface temperature, greenhouse gas concentration, and the representation of radiative transfer. We further show that the shifting ozone profile associated with climate warming may give rise to a fixed tropopause temperature as well as a fixed anvil temperature. This result points to the importance of faithful treatment of ozone in simulating clouds and climate change; the robust anvil-tropopause relationship may also provide alternative ways to understand what controls anvil temperature.

1. Introduction

The tropical upper troposphere is home to extensive cirrus clouds detrained from thunderstorms. As the surface warms, these clouds – known as anvil clouds – are robustly predicted to rise to greater altitudes so that their mean temperature increases less than that of the surface. This holds true in cloud-resolving models (CRMs) (Tompkins and Craig 1999; Kuang and Hartmann 2007; Harrop and Hartmann 2012; Khairoutdinov and Emanuel 2013; Narenpitak et al. 2017) general circulation models (GCMs) (Zelinka and Hartmann 2010; Thompson et al. 2017), as well as observations (Zelinka and Hartmann 2011). Since anvil clouds' temperature changes little under surface warming, they will emit less longwave radiation to space than if they were to warm at the same rate as the surface. This yields a positive climate feedback when our reference assumption is that clouds should otherwise warm at the same rate as the surface. For this reason, the most recent IPCC report expressed *high confidence* in a positive longwave cloud altitude feedback (Forster et al. 2021).

The Fixed Anvil Temperature (FAT) hypothesis is the most enduring explanation for the trend of high-cloud temperature with surface warming (Hartmann and Larson 2002). The FAT hypothesis claims that (1) upper tropospheric cloud amount is principally the result of the radiatively-driven horizontal convergence in clear skies, and (2) this convergence is physically constrained to occur at a fixed temperature. Indeed, studies of CRMs, GCMs, and observations corroborate the first claim. The upper tropospheric maximum in convergence covaries with the upper tropospheric

maximum in cloud amount (Kuang and Hartmann 2007; Zelinka and Hartmann 2010; Bony et al. 2016; Seeley et al. 2019b; Zelinka and Hartmann 2011). However, models often contradict the second claim in FAT, showing that anvils and the location of maximum convergence may in fact warm appreciably, albeit slowly compared to the surface. For example, Kuang and Hartmann (Kuang and Hartmann 2007) showed in a CRM that the location of maximum cloud fraction to warm by 2 K when the surface warmed by 8 K, and the recent Radiative-Convective Equilibrium Model Intercomparison Project found an average of 4.4 K of anvil warming over 10 K of surface warming (Wing et al. 2020). This slow but appreciable warming is sometimes known as a Proportionately Higher Anvil Temperature, or PHAT. PHAT may be explained considering the changing static stability profile of the upper troposphere under climate warming (Zelinka and Hartmann 2010; Harrop and Hartmann 2012). Importantly, even a PHAT gives rise to a positive cloud altitude feedback.

It is sometimes assumed that anvil clouds are linked to the radiative tropopause, where radiative heating first goes to zero in the upper troposphere (see, e.g., Birner and Charlesworth 2017; Kluft et al. 2019). Radiative tropopause is the intersection of the radiative-convective equilibrium (RCE) temperature profile of the troposphere and the radiative equilibrium profile of the stratosphere (Vallis et al. 2015; Hu and Valliss 2019). Since radiative tropopause is the highest location convection reaches in RCE, it is also known as the convective top (Thuburn and Craig 2002; Birner and Charlesworth 2017; Dacie et al. 2019). Tompkins and Craig (Tompkins and Craig 1999) found in a CRM that anvil temperature to increase with surface warming. They suggested this occurred because the tropopause temperature increases with warming due to their fixed ozone profile. Kluft et al. (2019) modeled radiative tropopause to warm by about 0.5 K per 1 K of surface warming using a 1-D RCE model without clouds. Assuming a close relationship between tropopause and anvil, the authors suggested that their result supported a PHAT. Such an assumption appears to be a crude simplification of FAT/PHAT thinking, according to which a decline in radiative cooling with height below tropopause causes clear-sky convergence.

Since radiative tropopause may be simulated by 1-D models without clouds, a robust anvil-tropopause relationship would simplify our understanding of anvil clouds. However, Seeley et al. (Seeley et al. 2019b) achieved a contrary result in CRM simulations of clouds and tropopause. In their simulations the temperature of radiative tropopause varied by less than 2 K despite 50 K of

surface warming, yet the anvil warming was greater by an order of magnitude. They suggested that not only is there a fixed tropopause temperature (FiTT) with respect to surface warming, but tropopause temperature is unlikely to be related to the temperature of the anvil peak. That is, the top of the troposphere should be disentangled from the anvil location. Given this disagreement and the potential clarity provided by an anvil-tropopause relationship, it is worthwhile to investigate more thoroughly whether the location and temperature anvil clouds are in fact related to the location and temperature of tropopause.

To test for an anvil-tropopause relationship, we conduct idealized experiments in a CRM systematically changing the radiation-relevant model settings. We ask: Do changes in model settings that change the simulated tropopause temperature cause similar changes in the anvil temperature? Are changes in the tropopause temperature's *trend* with respect to surface warming associated with similar changes in the anvil temperature trend? In particular, we test the sensitivity of anvil and tropopause temperature to: (1) A wide range of surface temperatures (280 K to 315 K); (2) the amount of carbon dioxide; (3) the amount of insolation; (4) the shape, concentration, and location of the ozone profile; (5) the presence of a large-scale circulation and convective organization; and (6) the domain size.

2. Simulations

We use the 2D formulation of the System for Atmospheric Modeling (SAM), version 6.10 (Khairoutdinov and Randall 2003). SAM is a cloud-permitting model using the anelastic equations for dynamics. 2D CRMs have long been used to study convection and clouds in the tropics (Held et al. 1993; Grabowski et al. 2000; Blossey et al. 2010; Yang 2018a,b; Seidel and Yang 2020). The horizontal resolution is 2 km. Radiation is parameterized using the Rapid Radiative Transfer Model (RRTM) (Mlawer et al. 1997). Cloud microphysics are parameterized using the SAM one-moment scheme. For the purposes of replicability and comparability, we borrowed many modeling parameters from the Radiative Convective Equilibrium Model Intercomparison Project (RCEMIP) protocol (Wing et al. 2018). The vertical grid is a modified version of the RCEMIP high-vertical-resolution grid, extended to allow for greater surface temperature. It consists of 160 levels, with a vertical resolution of 40m at the surface, 200m at altitudes between 3 km and 25 km, and increasing to 500m above that. The model top is at 36 km. A sponge layer occupies the upper 30% of the model domain. To accommodate the computational cost of exploring a wide range of modeling

conditions, as well as the long equilibration times required, our standard simulations use a small, 256 km domain. To test the relevance of convective organization, we use a larger 2048 km domain. Following RCEMIP, we use an idealized equatorial ozone profile and CH_4 and N_2O concentrations of 1650 and 306 ppbv, respectively. Insolation is fixed at 409.6 W/m^2. Unlike the RCEMIP protocol, we set CO_2 to its preindustrial value of 280 ppmv. All other well-mixed greenhouse gases are set to zero.

The model is run over a sea surface with a prescribed temperature until the atmosphere approximately reaches radiative-convective equilibrium (RCE). RCE is an idealization of the tropical atmosphere which states that the latent heating from convection is balanced by radiative cooling in the free troposphere. Each simulation is integrated for 500 days, except for simulations without ozone, which required 1000 days to equilibrate. The data reported are from the final 40% of the model integration. We identify cloudy grid cells as those whose condensates exceed either $1x10^{-5}\ kg/kg$ or 1% of the saturation specific humidity, whichever is smaller. This is consistent with the method of the RCEMIP protocol as well as SAM's own diagnostic code. Even for small domains, SAM has a high propensity to undergo convective self-aggregation, in which convection spontaneously organizes into persistent moist and dry patches (Tompkins 2001; Bretherton et al. 2006; Held et al. 1993). To prevent this, we horizontally homogenize radiation in all simulations except for a single set of large-domain simulations meant to test the importance of organization. Each "experiment" in this study consists of eight simulations with prescribed sea-surface temperatures from 280 K to 315 K. We present twelve experiments in total, variously adjusting the CO_2 concentration, the insolation, and the ozone profile. These experiments are summarized in Table 1.

Experiment	Domain	Ozone	Insolation	CO_2
Standard	256 km	Standard	409.6 W/m^2	280 ppm
Standard, 4xCO_2	256 km	Standard	409.6 W/m^2	1120 ppm
Standard, no CO_2	256 km	Standard	409.6 W/m^2	0 ppm
No Solar	256 km	Standard	0 W/m^2	0 ppm
2x Solar	256 km	Standard	819.2 W/m^2	0 ppm
Unif-O_3	256 km	Uniform	409.6 W/m^2	0 ppm
Unif-O_3-no-Solar	256 km	Uniform	0 W/m^2	0 ppm
1/10 O_3	256 km	0.1 x Standard	409.6 W/m^2	0 ppm
No O_3	256 km	None	409.6 W/m^2	280 ppm
Large	2048 km	Standard	409.6 W/m^2	280 ppm
Large-Organized*	2048 km	Standard	409.6 W/m^2	280 ppm
CAM Radiation*	256 km	Standard	409.6 W/m^2	280 ppm

Table 1. Summary of all idealized experiments conducted in this study. Each experiment consists of 8 simulations with prescribed surface temperatures of 280 K, 285 K, 290 K, 295 K, 300 K, 305 K, 310 K, and 315 K. The Large-Organized experiment is conducted without homogenized radiation. The CAM Radiation experiment is conducted using the CAM3 radiation scheme rather than RRTMG.

120

121 ## 3. Results

122 As the climate warms, anvil clouds rise in altitude so that their temperature increases less than the
123 air at any given level. Figure 1a shows profiles of cloud fraction from the Standard simulations
124 (see Table 1). The cloud fraction profile has a two-peaked structure. Following the convention of
125 other studies (Kuang and Hartmann 2007; Wing et al. 2020), we refer to upper-tropospheric peak
126 in cloud fraction as the anvil, which migrates upward as the surface warms. Figure 1b shows cloud

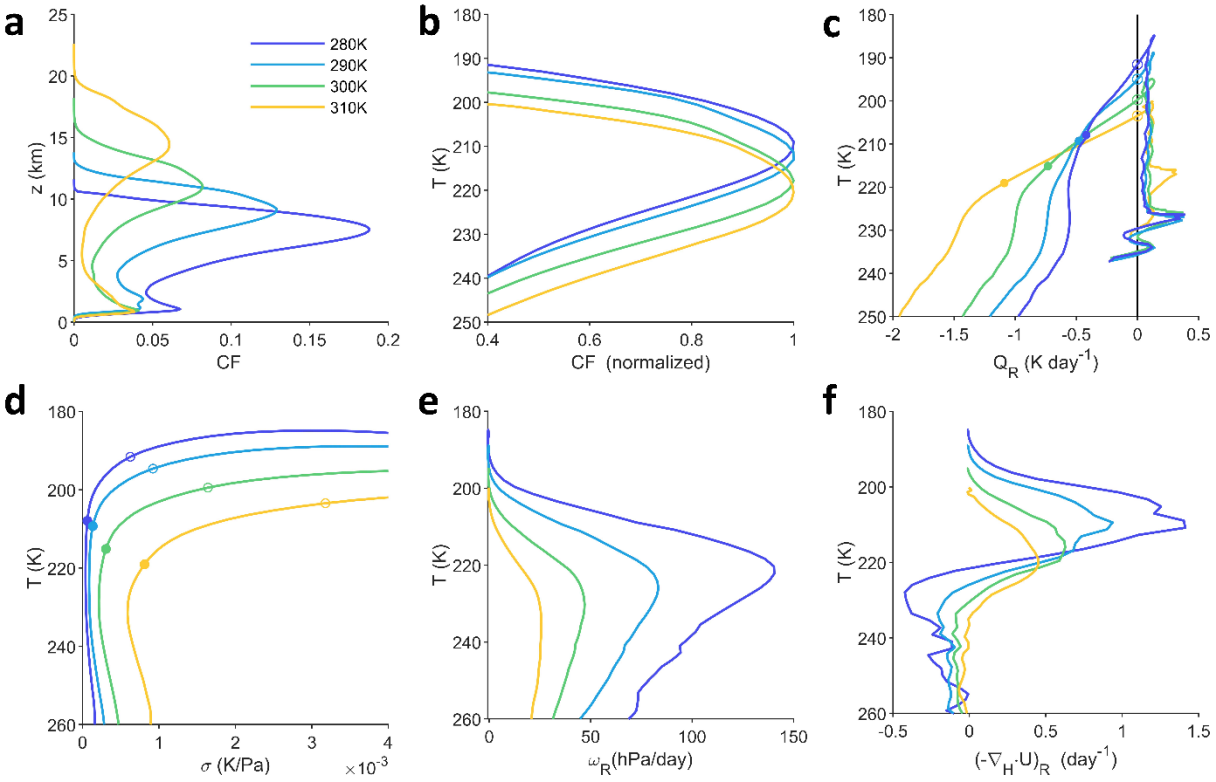

Figure 1. The Standard experiment. (a) Profiles of cloud fraction from the Standard simulations. (b) Cloud fraction, normalized by its maximum value, and plotted against temperature. (c) Radiative heating plotted against temperature. The open circles on the y-intercept indicate radiative tropopause. The closed circles indicate the location of T_{conv}. (d) Static stability profiles. The open circles indicate radiative tropopause. The closed circles indicate T_{conv}. (e) Radiatively driven subsidence. (f) Radiatively driven convergence.

fraction on a temperature coordinate and normalized by dividing by its local maximum value. The anvil temperature increases with warming.

We require a precise and general definition of "anvil temperature" appropriate for the wide range of surface temperature and physics perturbations in this study. Defining anvil to be the temperature where the cloud fraction reaches its maximum value (Kuang and Hartmann 2007; Seeley et al.

2019b; Wing et al. 2020) proved inadequate for some of our experiments. The temperature of maximum cloud fraction may shift dramatically with warming due to a modest change in cloud shape, rather than a meaningful change in high-cloud temperature (Fig. S1). Using a cloud-mass-weighted temperature over the entire portion of the troposphere below a certain temperature (Zelinka and Hartmann 2010; Harrop and Hartmann 2012) is also not adequate for our experiments. Given the wide range of surface temperatures in our experiments, there isn't a single temperature or pressure level consistently demarcating the "upper troposphere" from the "lower troposphere". To avoid these shortcomings, we first identify the upper-tropospheric peak in cloud fraction. Then we calculate a cloud-mass-weighted temperature over the locations where cloud coverage of at least 80% of that maximum value:

$$T_{anv} = \int_{p_{80\%,\uparrow}}^{p_{80\%,\downarrow}} T(p) \cdot CF(p)\, dp \tag{1}$$

where T is temperature, CF is cloud fraction, and $p_{80\%,\uparrow}$ and $p_{80\%,\downarrow}$ are the highest and lowest pressure levels where the cloud fraction is at least 80% of its maximum value. This cutoff is arbitrary choice, but in the supplemental material we show that Eq. (1) gives nearly the same temperature as a strict "peak" definition except in a few cases where the shape of the cloud profile changes abruptly with warming (Fig. S2). In those cases Eq. (1) retains monotonic behavior rather than allowing an arbitrary jump in T_{anv}. Therefore, this method is more appropriate for this study. To reduce the imprecision introduced by a discrete model resolution, we linearly interpolate $T(p)$ and $CF(p)$ in pressure and calculate the integral in Eq. (1) numerically.

Figure 2 shows T_{anv} for each experiment in this study. In the Standard simulations, anvil temperature (T_{anv}) increases by 13.2 K while the surface temperature (T_s) increases by 35 K, so that $\Delta T_{anv}/\Delta T_s = 0.38$. The anvil warms appreciably albeit more slowly than the surface, which

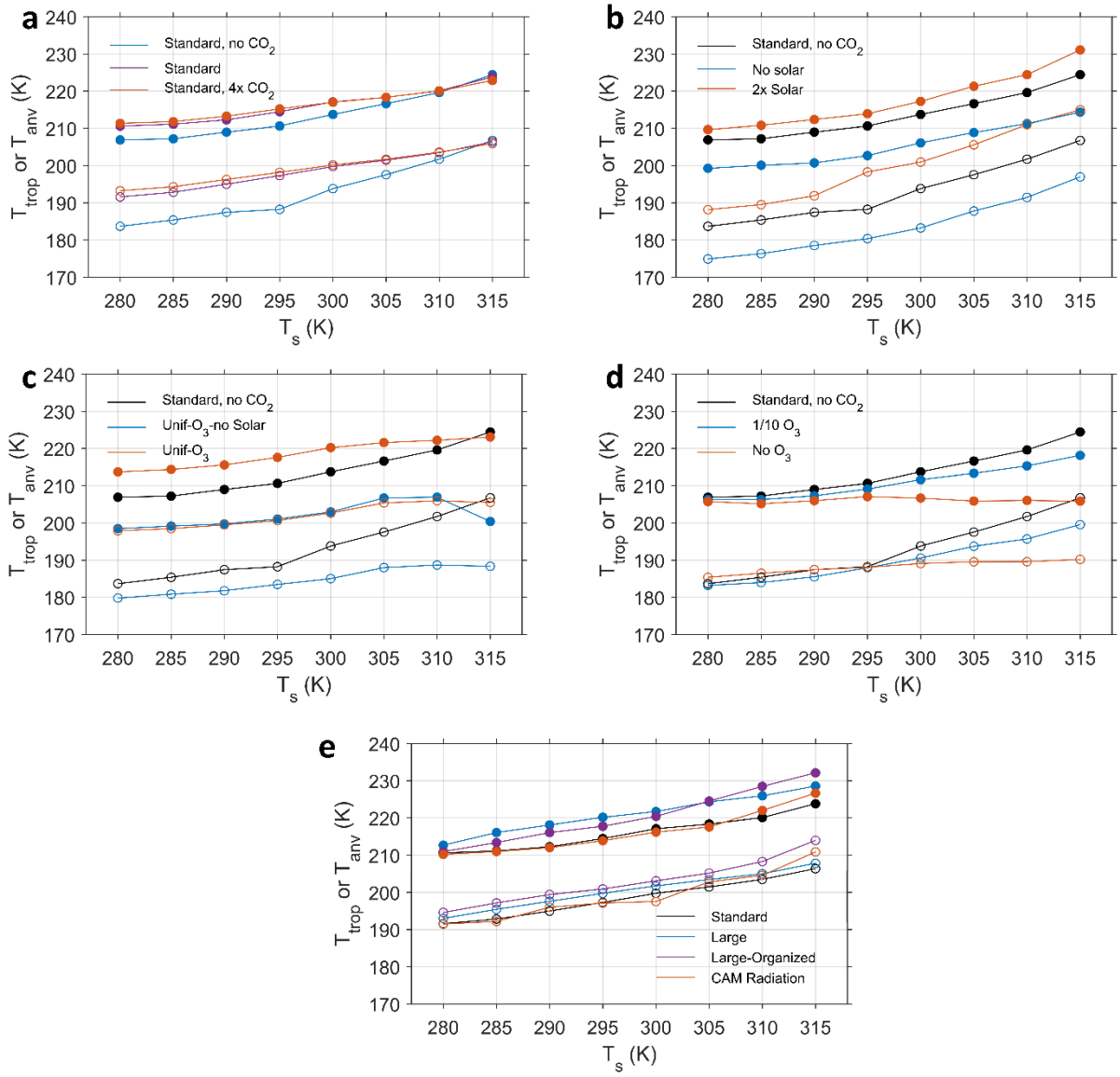

Figure 2. Tropopause and anvil temperatures. Tropopause temperature (open circles) and anvil temperature (closed circles) for each simulation used in this study. Black lines and marks indicate a simulation, also present in another panel, used as a baseline for comparison.

agrees with previous CRM and GCM studies. (Kuang and Hartmann 2007; Zelinka and Hartmann 2010; Harrop and Hartmann 2012; Khairoutdinov and Emanuel 2013). RCEMIP, whose protocol forms the basis for our experimental design, showed an average anvil warming of $\Delta T_{anv}/\Delta T_s = 0.44$ (Wing et al. 2020). By replicating the results of 3D CRMs, we affirm that a 2D CRM is appropriate for investigating anvil temperature.

As the climate warms, the radiative tropopause becomes warmer as well. Figure 1c shows radiative heating using temperature as a vertical coordinate. Considering the troposphere as the region of the atmosphere in radiative-convective equilibrium, we identify radiative tropopause as the temperature at which radiative heating changes sign. That is, tropopause is the y-intercept in Fig. 1c, marked with an open circle for each simulation. The tropopause temperature for the Standard experiment is shown in Fig. 2a. Tropopause temperature (T_{trop}) increases by 14.8 K over a 35 K increase in T_s, so that $\Delta T_{trop}/\Delta T_s = 0.42$. This replicates recent studies of radiative-convective equilibrium in 1-D models without clouds. Kluft et al. (2019) showed $\Delta T_{trop}/\Delta T_s \approx 0.5$, and they noted that the temperature increase of radiative tropopause (or "convective top") resembled the slow temperature increase of anvil clouds. Dacie et al. (2019) similarly showed $\Delta T_{trop}/\Delta T_s \approx 0.4$, though they defined radiative tropopause as the threshold where convective heating (or radiative cooling) equals 0.2 K/day.

We examine the relationship between the anvil and tropopause temperatures using a variety of modeling choices. We ask: do anvil temperature and tropopause temperature covary in response to a change of model parameters? Figure 2a shows the results from three simulations: the Standard experiment; the Standard, 4xCO_2 experiment; and the Standard, no CO_2 experiment. When CO_2 is quadrupled, tropopause temperature increases more slowly with surface warming ($\Delta T_{trop}/\Delta T_s = 0.36$) than the Standard simulation. On the other hand, when CO_2 is removed entirely, tropopause temperature increases more rapidly with surface warming ($\Delta T_{trop}/\Delta T_s = 0.66$). In either case, the trend in anvil temperature mirrors that of tropopause temperature: increasing CO_2 slightly decreases the trend with warming ($\Delta T_{anv}/\Delta T_s = 0.33$), while removing CO_2 allows the anvil to warm much more over the course of the simulations ($\Delta T_{anv}/\Delta T_s = 0.50$). Therefore, the anvil and tropopause appear to be related.

Solar radiation also has a substantial effect on anvil and tropopause temperature. Figure 2b shows experiments in which we either double incoming solar radiation (2x Solar) or remove it entirely (No Solar). With solar radiation reduced from an Earthlike value to zero, the anvil and tropopause temperatures each become about 10 K colder. When solar radiation is doubled, they each become about 5 K warmer. However, the differences in warming trends $\Delta T_{trop}/\Delta T_s$ and $\Delta T_{anv}/\Delta T_s$ between the three experiments are modest. As with the CO_2 experiments, the perturbations in anvil temperature mirror the perturbations in tropopause temperature.

Finally, we conduct four experiments in which we manipulate the ozone profile. In the Unif-O_3 and Unif-O_3-no-Solar, experiments, we prescribe ozone as vertically uniform over the depth of the domain, while maintaining the same column mass of ozone as in the other simulations. The results of these experiments are shown in Fig. 2c. In the Unif-O_3 experiment, the temperature trends are $\frac{\Delta T_{trop}}{\Delta T_s} = 0.22$, and $\frac{\Delta T_{anv}}{\Delta T_s} = 0.27$, both smaller compared to the Standard-no-CO2 experiment. Curiously, for both these experiments and the standard-ozone experiments presented in Fig. 2b, the trends $\Delta T_{trop}/\Delta T_s$ and $\Delta T_{anv}/\Delta T_s$ are not especially sensitive to the presence of solar radiation. The shape and magnitude of the ozone profile are more important than whether its principal action is in the shortwave or longwave bands.

In two other experiments, shown in Fig. 2d, we change the concentration of ozone. The 1/10 O_3 experiment is identical to the Standard-no CO_2 experiment except with ozone reduced to 10% of its RCEMIP value while maintaining its shape. The tropopause's and anvil's trends with warming are reduced compared to the Standard-no CO_2 experiment. In the No O_3 experiment we remove ozone entirely and instead add 280 ppm of CO_2 to serve as a radiatively active gas in the stratosphere.[1] When ozone is eliminated, the tropopause warms less than in any other experiment ($\Delta T_{trop}/\Delta T_s = 0.14$), and the anvil temperature is approximately fixed ($\Delta T_{anv}/\Delta T_s = 0.01$). For the No O_3 experiment, the anvil temperature is especially sensitive to which portion of the cloud we define as the "anvil", so this result should be considered with caution (see Fig. S2d).

Our assumptions about ozone have a profound effect on the simulated trends of anvil and tropopause temperature. The RCEMIP ozone profile is based on the equatorial climatology so that it increases with height in the upper troposphere and lower stratosphere. Thus, when the surface warms, the troposphere is being lifted into an increasing ozone concentration. When ozone is homogenized or eliminated, this mechanism is no longer present, and the tropopause and anvil warm much more slowly as the surface warms. These results resemble those of Harrop and Hartmann (2012), who found that removing ozone nearly eliminated any trend in anvil temperature. However, Seeley et al. (2019b) simulated a PHAT in the absence of ozone. That

[1] Following Harrop and Hartmann (Harrop and Hartmann 2012) and Seeley et al. (Seeley et al. 2019b), we also attempted simulations removing both ozone and CO_2. However, even over long equilibration times (>1000 days), the top of the model never stabilized to a steady temperature, and the simulations failed as temperatures there became unrealistically cold. Adding a radiatively active, non-condensable gas (in this case CO_2) resolved this problem.

study, as well as an earlier study by Jeevanjee and Romps (2018), also found a nearly fixed tropopause temperature ($\Delta T_{trop}/\Delta T_s = 0.04$ in Seeley et al.) This led Seeley et al. to propose a fixed tropopause temperature (FiTT). Our No O_3 experiment's tropopause trend $\Delta T_{trop}/\Delta T_s$ is the smallest of any experiment we perform, which we interpret to be consistent with Seeley et al. (though their tropopause temperature was much more strictly fixed). We shall revisit ozone later in the article.

Finally, we verify that our choice of a small modeling domain and lack of convective organization do not affect our earlier conclusions. Figure 2e shows the anvil and tropopause temperatures for the two large-domain experiments, as well as the Standard experiment. In one experiment the radiative heating is horizontally homogenized, preventing convective organization, and in the other radiation is interactive to allow organization. Compared to the standard, small-domain simulations presented in Fig. 1 and depicted by the black marks in Fig. 2e, the anvil temperature and tropopause temperature are both slightly warmer but display otherwise similar trends with warming. Convective organization does not appear to affect anvil temperature, consistent with previous studies (Wing et al. 2020; Harrop and Hartmann 2012). Another experiment using the CAM3 radiation scheme (Collins et al. 2006) demonstrates that there is only small sensitivity to our choice of radiation parameterization.

Throughout our experiments, we find that the temperature of the cloud anvil is empirically related to the temperature of radiative tropopause. Figure 3a shows the anvil temperature plotted against the tropopause temperature for each simulation we conducted. Anvil and tropopause always occur at different locations and temperatures from one another, yet they appear closely related. If a simulation results in a warmer tropopause, then it generally yields a warmer anvil. The anvil-tropopause relationship is robust over 96 simulations in a wide range of model settings. This is our central result.

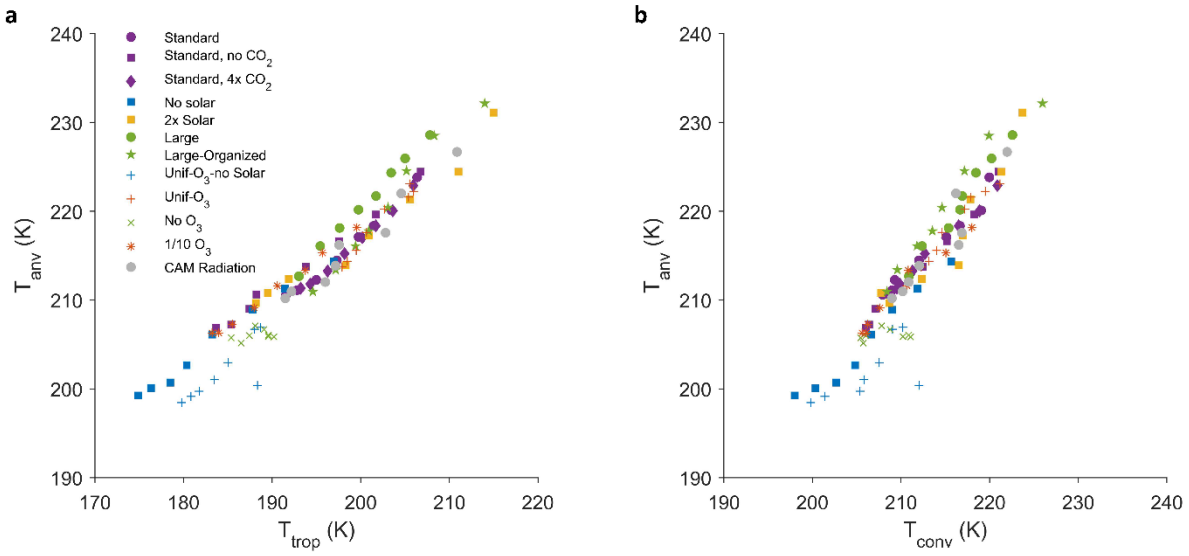

Figure 3. Relationship between T_{trop} and T_{anv}. (A) T_{anv} plotted against T_{trop} for each simulation in this study. (B) T_{anv} plotted against T_{conv} for each simulation in this study.

238 *a. Radiatively-Driven Convergence*

239 The cloud fraction profile is the result of sources and sinks of cloudy air: detrainment from the
240 convective core and evaporation into the environment, respectively (Seeley et al. 2019a). We focus
241 on one component of the sources, due to the radiatively driven subsidence of air in clear skies
242 (Kuang and Hartmann 2007; Zelinka and Hartmann 2010):

$$\omega_R = -\frac{Q_R}{\sigma} \tag{2}$$

243 Here, ω_R is a pressure velocity (Pa/day), Q_R is the radiative heating rate (K/day) and σ is the
244 static stability (K/Pa), given by:

$$\sigma = \frac{\Gamma_d - \Gamma}{\rho g} \tag{3}$$

245 Where Γ is the lapse rate (K/m), Γ_d is the dry-adiabatic lapse rate, ρ is density, and g is the
246 acceleration due to gravity. The radiatively driven horizontal convergence of air in clear skies is
247 then given by:

$$(-\nabla_{\mathrm{H}} \cdot \mathbf{U})_R = \partial \omega_R / \partial p \quad (4)$$

In the absence of mean ascent or subsidence over the domain, $(-\nabla_{\mathrm{H}} \cdot \mathbf{U})_R$ is balanced by divergence out of the convective region at the same altitude. Past modeling studies found that the peak upper-tropospheric cloud fraction tends to be located at or near the maximum in $(-\nabla_{\mathrm{H}} \cdot \mathbf{U})_R$ (Kuang and Hartmann 2007; Zelinka and Hartmann 2010; Seeley et al. 2019b).

The radiative heating rate Q_R from the Standard experiment is shown in Fig. 1c. Since radiation is horizontally homogenized in our simulations, we use domain-averaged values of Q_R in our calculation. Figures 1d and 1e show σ and ω_R, plotted against a temperature coordinate. The static stability σ increases with height as the atmosphere transitions from a radiative-convective equilibrium temperature profile below to a more stable radiative equilibrium profile above. This transition to greater static stability is coincident with a steady decline in the magnitude of Q_R toward the radiative tropopause. Therefore, ω_R declines sharply with altitude at that level. The peak in radiative convergence $(-\nabla_{\mathrm{H}} \cdot \mathbf{U})_R$ occurs there, as shown in Fig. 1f. The peak in $(-\nabla_{\mathrm{H}} \cdot \mathbf{U})_R$ moves to a higher temperature as the surface temperature increases, much like the cloud fraction in Fig. 1b. The magnitude of $(-\nabla_{\mathrm{H}} \cdot \mathbf{U})_R$ also declines, primarily due to increasing σ. This matches a decline in anvil cloud extent seen in Fig. 1a, consistent with the "stability iris" hypothesis described by Bony et al. (Bony et al. 2016).

The relationship among tropopause temperature, convergence temperature, and anvil temperature is robust across all the experiments in this study. We define a convergence-weighted temperature similar to how we defined an anvil temperature before: $T_{conv} = \int_{p_{80\%,\uparrow}}^{p_{80\%,\downarrow}} T(p) \cdot \frac{\partial \omega_R}{\partial p}(p)\, dp$, where $p_{80\%,\uparrow}$ and $p_{80\%,\downarrow}$ are the highest and lowest pressure levels where $(-\nabla_{\mathrm{H}} \cdot \mathbf{U})_R$ is at least 80% of its maximum value. Figure 3b shows the relationship between this convergence-weighted temperature and anvil temperature. As found by previous studies of CRMs, GCMs, and observations, the temperature of cloud anvils is well-predicted by the convergence temperature. The empirical relationship between tropopause temperature, anvil temperature, and convergence temperature suggests that anvil and tropopause arise from related physics. Insofar as radiative tropopause lies above a rapid decline in Q_R with height or an increase in σ with height, then large values of radiatively driven convergence may be found there via Eqs. (2) and (4). However, any prospective explanation of the anvil-tropopause relationship must account for the distance between

the tropopause (open circles in Figs. 1c and 1d) and the location of maximum radiatively-driven convergence (closed circles in Figs. 1c and 1d).

b. Tug of war: rising O_3 profiles vs. surface warming

Our Standard simulations used an ozone profile which is fixed in pressure despite a warming surface. This is unrealistic. In the real tropical atmosphere, the ozone profile should evolve in response to the changing location of tropopause as tropospheric mixing reduces ozone. Additionally, upward transport of ozone may increase as stratospheric upwelling intensifies with surface warming (Lin et al. 2017). This will alter the equilibrium tropopause temperature, as ozone is the main absorber responsible for radiative heating there (Thuburn and Craig 2002). As shown in our simulations, surface warming leads to a warmer tropopause with a fixed O_3 profile. However, lifting the O_3 profile can lead to the local decline of ozone heating, which tends to reduce temperature. Therefore, there is a "tug of war" between the two effects to determine how tropopause temperature responds to climate warming in the real tropical atmosphere. Thus, we cannot predict anvil or tropopause's temperature trend with warming using a fixed ozone profile.

To investigate the role of ozone, past studies have artificially increased upper-tropospheric ozone, leading to greater anvil temperature (Kuang and Hartmann 2007) as well as greater tropopause temperature (Birner and Charlesworth 2017; Dacie et al. 2019). Other authors have simply removed ozone entirely, as in our No O_3 experiment (Jeevanjee and Romps 2018; Seeley et al. 2019b; Harrop and Hartmann 2012). However, those idealized treatments of the ozone profile cannot provide a quantitative estimate of how ozone influences the warming trend of anvil or tropopause. Does the rising troposphere or declining ozone concentration win the tug of war, or do they cancel one another? To answer that question, we shall prescribe ozone from the Whole Atmosphere Community Climate Model (CESM2-WACCM6), which employs coupled ozone chemistry (Gettelman et al. 2019).

We use WACCM6 data from a pre-industrial control run in which the CO_2 concentration is fixed at 280 ppm ("piControl"), as well as a simulation of the surface and atmosphere's response to an abrupt quadrupling of CO_2 concentration ("abrupt-4xCO2") (Eyring et al. 2016; Danabasoglu 2019). For either simulation we average the final 50 years of data, within 10 degrees of the equator. In that region, tropical sea surface temperature increases from 301.21 K at the end of the piControl

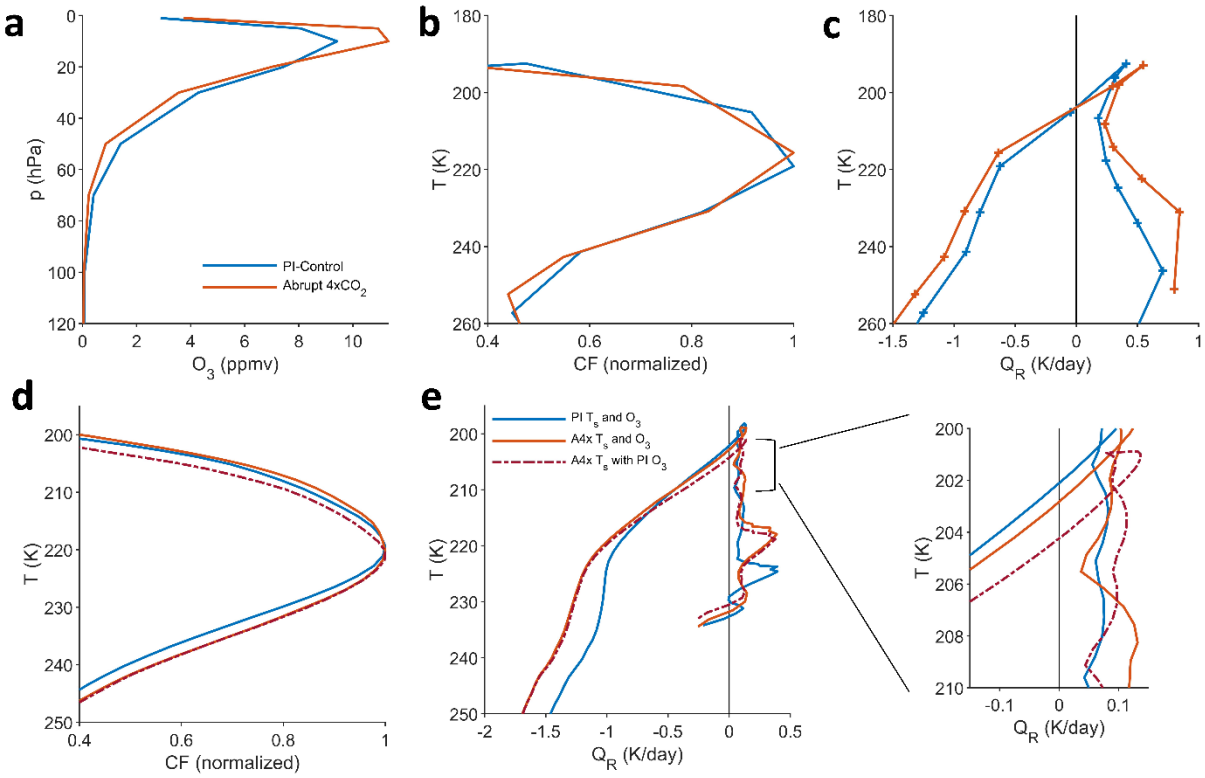

Figure 4. CESM2-WACCM simulations and WACCM-informed SAM simulations. (a) CESM2-WACCM ozone. (b) Cloud fraction plotted against a temperature coordinate. (c) Radiative heating plotted against temperature. (d) Normalized cloud fraction for the SAM simulations based on WACCM surface temperature and ozone. (e) Radiative heating for the SAM simulations based on WACCM surface temperature and ozone.

simulation to 306.65 K at the end of the abrupt-4xCO2 simulation. Figure 4a shows that the ozone concentration decreases below the 20 hPa level and increases above. The ozone profile shifts

upward as the surface warms. Figure 4b shows that the normalized cloud profiles are nearly the same in a temperature coordinate.[2] WACCM simulates a FAT in the deep tropics. Figure 4c shows that WACCM simulates a FiTT in the deep tropics: tropopause temperature increases by only 0.05 K. The coarse resolution and small surface temperature increment of the GCM output undercut the precision of this estimate, but it is nevertheless a striking result.

To what extent does the shifted ozone profile account for the apparent temperature-invariance of the WACCM tropopause and anvil clouds? We modify our Standard formulation of 2D SAM. We conduct one simulation with the piControl surface temperature and ozone profile and a second simulation with the abrupt-4xCO2 surface temperature and ozone profile. As a mechanism-denial experiment, we conduct a third simulation with the warmer abrupt-4xCO2 surface temperature, but the lower piControl ozone profile. Unlike the GCM simulation, we fix CO_2 at 280ppm to isolate only the direct effects of surface temperature and ozone.

Figure 4d shows the cloud fraction profiles of the WACCM-informed SAM simulations. With ozone prescribed to match the surface temperature, the cloud fraction profile is nearly unchanged with respect to temperature. T_{anv}, calculated according to Eq. (1). increases by 0.4 K so that $\Delta T_{anv}/\Delta T_s = .07$. When ozone is instead fixed, T_{anv} increases by 1.5 K so that $\Delta T_{anv}/\Delta T_s = .28$. Figure 4e shows the radiative heating profiles of all three simulations. When ozone matches the surface temperature, T_{trop} increases by 0.7 K so that $\Delta T_{trop}/\Delta T_s = .13$. When ozone is instead fixed, T_{trop} increases by 2.1 K so that $\Delta T_{trop}/\Delta T_s = .39$. The ozone-shifted results resemble the idealized No-O_3 experiment presented earlier. For both anvil and tropopause, the shifted ozone profile offsets most of the warming that would occur with fixed ozone. Therefore, we find it plausible that the effects of increasing surface temperature and a lifted ozone profile roughly cancel one another to produce a FiTT as well as a FAT in the real atmosphere.

4. Discussion

We have shown that the temperatures of cloud anvils and radiative tropopause strongly covary across a wide range of model settings and surface temperatures in a 2D cloud-resolving model.

[2] T_{anv} as calculated from Eq. (1) decreases from 217.2 K to 216.6 K. However, due to the coarseness of the GCM output, the sign and magnitude of that change depend non-monotonically on what percentage threshold we consider as the "anvil" in that formula.

This affirms the commonly held intuition that anvils simply occur near the top of the troposphere where the radiative cooling rate declines towards zero. Our result is significant in light of a recent contrary result. Seeley et al. (Seeley et al. 2019b) found that anvil temperature increased in spite of a fixed tropopause temperature in CRM simulations without ozone. We did not replicate that result exactly, but the anvil-tropopause relationship is least robust in our experiment without ozone (see Figs. S2 & S3 for results using different definitions of the anvil temperature). This suggests that ozone heating – from solar radiation as well as absorption in the longwave water vapor window – may be essential to the anvil-tropopause relationship. In our Standard simulations the distance between anvil and tropopause is 2-3 km, substantially less than the 5-10 km reported by Seeley et al. Insofar as modeling choices or actual physics place the anvil further from tropopause, their respective temperatures may become decoupled. Additionally, while the anvil temperature tends to track with the tropopause temperature, their trends do not always correspond one-to-one in our simulations. This is most apparent in Fig. 2a. When CO_2 is removed, the modeled tropopause temperature declines more than anvil temperature. Even though anvil and tropopause appear to be related phenomena, we should be cautious of conflating the two.

We also find that the anvil temperature closely matches the temperature of maximum radiatively driven clear-sky convergence in the upper troposphere. This is consistent with the conventional understanding that detrainment due to clear-sky convergence is principally responsible for the location of anvil clouds. It is also consistent with an explanation offered by Seeley et al. (Seeley et al. 2019a): anvil clouds reach their maximum extent where the decline in detrainment with height overtakes the increase in cloud lifetimes with height due to slow evaporation. If radiatively-driven convergence is the principal cause of detrainment, and it declines sharply above its peak, then the anvil will appear there. In either case, this agreement with the previous literature suggests that our choice of a 2D CRM does not significantly compromise the relevance of our results.

Our WACCM-informed simulations, in which the ozone profile was lifted to match the surface temperature, showed that tropopause temperature may in fact be nearly fixed. Notably, GCMs typically show temperature to be increasing in the tropical tropopause layer temperature, while observations show it to be modestly declining (Thompson and Solomon 2005; Cordero and Forster 2006; Gettelman et al. 2010; Emanuel et al. 2013). This bias has been attributed to the prescribed ozone profiles typically used in GCMs, among other factors. Insofar as the tropopause layer is

biased towards warming in GCMs, then our results suggest the anvil temperature may also be biased towards warming. This would introduce a negative bias in cloud longwave feedback. Indeed, Nowack et al. (Nowack et al. 2015, 2018b) found that a prescribed, fixed ozone profile reduced tropical upper tropospheric clouds in GCM simulations of climate warming, yielding difference of about -0.1 $W/m^2/K$ in cloud longwave feedback compared to simulations with interactive ozone. The representation of clouds may be improved in models if ozone can respond to the rising tropopause, as suggested in recent literature (Nowack et al. 2018a; Hardiman et al. 2019).

Finally, we mention several caveats to this study. To afford the computational expense of conducting 99 five-hundred-day simulations, we use a small, two-dimensional domain. We prescribe no mean ascent or descent, whereas real tropical anvil clouds form in the context of mean ascent in both the troposphere and stratosphere. Our analysis relates cloud amount to the radiatively driven convergence in clear skies. However, that is not a closed budget for cloud amount. Other factors are known to cause detrainment from the convective core, and cloud amount further depends on its lifetime after detrainment (Seeley et al. 2019a,b). As with other studies on this topic, we only consider the temperature of the cloud near its peak amount, not its effective radiating temperature, which may be different.

Acknowledgements:

We acknowledge the World Climate Research Programme and its Working Group on Coupled Modelling, which coordinated and promoted CMIP6. We thank the Earth System Grid Federation (ESGF) for archiving the data and providing access, and the multiple funding agencies who support CMIP6 and ESGF. Computational resources were provided by the Department of Energy's National Energy Research Sceintific Computing Center (NERSC). SAM was provided by M. Khairoutdinov (http://rossby.msrc.sunysb.edu/~marat/SAM.html).

Data Availability Statement:

Model output used to achieve these results can be found at the UC Davis Box website. Additional data related to this paper may be requested from the authors.

5. References

Birner, T., and E. J. Charlesworth, 2017: On the relative importance of radiative and dynamical heating for tropical tropopause temperatures. *J. Geophys. Res.*, **122**, 6782–6797, https://doi.org/10.1002/2016JD026445.

Blossey, P. N., Z. Kuang, and D. M. Romps, 2010: Isotopic composition of water in the tropical tropopause layer in cloud-resolving simulations of an idealized tropical circulation. *J. Geophys. Res. Atmos.*, **115**, https://doi.org/10.1029/2010JD014554.

Bony, S., B. Stevens, D. Coppin, T. Becker, K. A. Reed, A. Voigt, and B. Medeiros, 2016: Thermodynamic control of anvil cloud amount. *Proc. Natl. Acad. Sci.*, **113**, 8927–8932, https://doi.org/10.1073/pnas.1601472113.

Bretherton, C. S., P. N. Blossey, and M. Khairoutdinov, 2006: An Energy-Balance Analysis of Deep Convective Self-Aggregation above Uniform SST. *J. Atmos. Sci.*, **62**, 4273–4292, https://doi.org/10.1175/jas3614.1.

Collins, W. D., and Coauthors, 2006: The formulation and atmospheric simulation of the Community Atmosphere Model version 3 (CAM3). *J. Clim.*, **19**, 2144–2161, https://doi.org/10.1175/JCLI3760.1.

Cordero, E. C., and P. M. D. F. Forster, 2006: Stratospheric variability and trends in models used for the IPCC AR4. *Atmos. Chem. Phys.*, **6**, 5369–5380, https://doi.org/10.5194/acp-6-5369-2006.

Dacie, S., and Coauthors, 2019: A 1D RCE study of factors affecting the tropical tropopause layer and surface climate. *J. Clim.*, **32**, 6769–6782, https://doi.org/10.1175/JCLI-D-18-0778.1.

Danabasoglu, G., 2019: *NCAR CESM2-WACCM model output prepared for CMIP6 CMIP abrupt-4xCO2*.

Emanuel, K., S. Solomon, D. Folini, S. Davis, and C. Cagnazzo, 2013: Influence of tropical tropopause layer cooling on atlantic hurricane activity. *J. Clim.*, **26**, 2288–2301,

https://doi.org/10.1175/JCLI-D-12-00242.1.

Eyring, V., S. Bony, G. A. Meehl, C. A. Senior, B. Stevens, R. J. Stouffer, and K. E. Taylor, 2016: Overview of the Coupled Model Intercomparison Project Phase 6 (CMIP6) experimental design and organization. *Geosci. Model Dev.*, **9**, 1937–1958, https://doi.org/10.5194/gmd-9-1937-2016.

Forster, P. M., and Coauthors, 2021: Chapter 7: The Earth's Energy Budget, Climate Feedbacks, and Climate Sensitivity. *Clim. Chang. 2021 Phys. Sci. Basis. Contrib. Work. Gr. I to Sixth Assess. Rep. Intergov. Panel Clim. Chang.*,.

Gettelman, A., and Coauthors, 2010: Multimodel assessment of the upper troposphere and lower stratosphere: Tropics and global trends. *J. Geophys. Res. Atmos.*, **115**, https://doi.org/10.1029/2009JD013638.

——, and Coauthors, 2019: The Whole Atmosphere Community Climate Model Version 6 (WACCM6). *J. Geophys. Res. Atmos.*, **124**, 12380–12403, https://doi.org/10.1029/2019JD030943.

Grabowski, W. W., J. I. Yano, and M. W. Moncrieff, 2000: Cloud resolving modeling of tropical circulations driven by large-scale SST gradients. *J. Atmos. Sci.*, **57**, 2022–2039, https://doi.org/10.1175/1520-0469(2000)057<2022:crmotc>2.0.co;2.

Hardiman, S. C., and Coauthors, 2019: The Impact of Prescribed Ozone in Climate Projections Run With HadGEM3-GC3.1. *J. Adv. Model. Earth Syst.*, **11**, 3443–3453, https://doi.org/10.1029/2019MS001714.

Harrop, B. E., and D. L. Hartmann, 2012: Testing the role of radiation in determining tropical cloud-top temperature. *J. Clim.*, **25**, 5731–5747, https://doi.org/10.1175/JCLI-D-11-00445.1.

Hartmann, D. L., and K. Larson, 2002: An important constraint on tropical cloud - climate feedback. *Geophys. Res. Lett.*, https://doi.org/10.1029/2002gl015835.

Held, I. M., R. S. Hemler, and V. Ramaswamy, 1993: Radiative-convective equilibrium with explicit two-dimensional moist convection. *J. Atmos. Sci.*, **50**, https://doi.org/10.1175/1520-0469(1993)050<3909:RCEWET>2.0.CO;2.

Hu, S., and G. K. Vallis, 2019: Meridional structure and future changes of tropopause height and temperature. *Q. J. R. Meteorol. Soc.*, **145**, 2698–2717, https://doi.org/10.1002/qj.3587.

Jeevanjee, N., and D. M. Romps, 2018: Mean precipitation change from a deepening troposphere. *Proc. Natl. Acad. Sci. U. S. A.*, **115**, 11465–11470, https://doi.org/10.1073/pnas.1720683115.

Khairoutdinov, M., and K. Emanuel, 2013: Rotating radiative-convective equilibrium simulated by a cloud-resolving model. *J. Adv. Model. Earth Syst.*, **5**, 816–825, https://doi.org/10.1002/2013ms000253.

Khairoutdinov, M. F., and D. A. Randall, 2003: Cloud Resolving Modeling of the ARM Summer 1997 IOP: Model Formulation, Results, Uncertainties, and Sensitivities. *J. Atmos. Sci.*, **60**, 607–625, https://doi.org/10.1175/1520-0469(2003)060<0607:CRMOTA>2.0.CO;2.

Kluft, L., S. Dacie, S. A. Buehler, H. Schmidt, and B. Stevens, 2019: Re-examining the first climate models: Climate sensitivity of a modern radiative–convective equilibrium model. *J. Clim.*, **32**, 8111–8125, https://doi.org/10.1175/JCLI-D-18-0774.1.

Kuang, Z., and D. L. Hartmann, 2007: Testing the fixed anvil temperature hypothesis in a cloud-resolving model. *J. Clim.*, **20**, 2051–2057, https://doi.org/10.1175/JCLI4124.1.

Lin, P., D. Paynter, Y. Ming, and V. Ramaswamy, 2017: Changes of the tropical tropopause layer under global warming. *J. Clim.*, **30**, 1245–1258, https://doi.org/10.1175/JCLI-D-16-0457.1.

Mlawer, E. J., S. J. Taubman, P. D. Brown, M. J. Iacono, and S. A. Clough, 1997: Radiative transfer for inhomogeneous atmospheres: RRTM, a validated correlated-k model for the longwave. *J. Geophys. Res. Atmos.*, **102**, 16663–16682, https://doi.org/10.1029/97jd00237.

Narenpitak, P., C. S. Bretherton, and M. F. Khairoutdinov, 2017: Cloud and circulation feedbacks in a near-global aquaplanet cloud-resolving model. *J. Adv. Model. Earth Syst.*, **9**, https://doi.org/10.1002/2016MS000872.

Nowack, P., P. Braesicke, J. Haigh, N. L. Abraham, J. Pyle, and A. Voulgarakis, 2018a: Using machine learning to build temperature-based ozone parameterizations for climate sensitivity simulations. *Environ. Res. Lett.*, **13**, https://doi.org/10.1088/1748-9326/aae2be.

Nowack, P. J., N. Luke Abraham, A. C. Maycock, P. Braesicke, J. M. Gregory, M. M. Joshi, A. Osprey, and J. A. Pyle, 2015: A large ozone-circulation feedback and its implications for global warming assessments. *Nat. Clim. Chang.*, **5**, https://doi.org/10.1038/nclimate2451.

——, N. L. Abraham, P. Braesicke, and J. A. Pyle, 2018b: The Impact of Stratospheric Ozone Feedbacks on Climate Sensitivity Estimates. *J. Geophys. Res. Atmos.*, **123**, https://doi.org/10.1002/2017JD027943.

Seeley, J. T., N. Jeevanjee, W. Langhans, and D. M. Romps, 2019a: Formation of Tropical Anvil Clouds by Slow Evaporation. *Geophys. Res. Lett.*, https://doi.org/10.1029/2018GL080747.

——, ——, and D. M. Romps, 2019b: FAT or FiTT: Are Anvil Clouds or the Tropopause Temperature Invariant? *Geophys. Res. Lett.*, https://doi.org/10.1029/2018GL080096.

Seidel, S. D., and D. Yang, 2020: The Lightness of Water Vapor Helps to Stabilize Tropical Climate. *Sci. Adv. Press*,.

Thompson, D. W. J., and S. Solomon, 2005: Recent stratospheric climate trends as evidenced in radiosonde data: Global structure and tropospheric linkages. *J. Clim.*, **18**, 4785–4795, https://doi.org/10.1175/JCLI3585.1.

——, S. Bony, and Y. Li, 2017: Thermodynamic constraint on the depth of the global tropospheric circulation. *Proc. Natl. Acad. Sci. U. S. A.*, **114**, 8181–8186, https://doi.org/10.1073/pnas.1620493114.

Thuburn, J., and G. C. Craig, 2002: On the temperature structure of the tropical substratosphere. *J. Geophys. Res. Atmos.*, **107**, https://doi.org/10.1029/2001jd000448.

Tompkins, A. M., 2001: Organization of tropical convection in low vertical wind shears: The role of water vapor. *J. Atmos. Sci.*, **58**, 529–545, https://doi.org/10.1175/1520-0469(2001)058<0529:OOTCIL>2.0.CO;2.

——, and G. C. Craig, 1999: Sensitivity of tropical convection to sea surface temperature in the absence of large-scale flow. *J. Clim.*, **12**, 462–476, https://doi.org/10.1175/1520-0442(1999)012<0462:SOTCTS>2.0.CO;2.

Vallis, G. K., P. Zurita-Gotor, C. Cairns, and J. Kidston, 2015: Response of the large-scale

500 structure of the atmosphere to global warming. *Q. J. R. Meteorol. Soc.*, **141**, 1479–1501,
501 https://doi.org/10.1002/qj.2456.

502 Wing, A. A., K. A. Reed, M. Satoh, B. Stevens, S. Bony, and T. Ohno, 2018: Radiative-
503 convective equilibrium model intercomparison project. *Geosci. Model Dev.*,
504 https://doi.org/10.5194/gmd-11-793-2018.

505 ——, and Coauthors, 2020: Clouds and Convective Self-Aggregation in a Multimodel Ensemble
506 of Radiative-Convective Equilibrium Simulations. *J. Adv. Model. Earth Syst.*,
507 https://doi.org/10.1029/2020MS002138.

508 Yang, D., 2018a: Boundary Layer Diabatic Processes, the Virtual Effect, and Convective Self-
509 Aggregation. *J. Adv. Model. Earth Syst.*, **10**, 2163–2176,
510 https://doi.org/10.1029/2017MS001261.

511 ——, 2018b: Boundary Layer Height and Buoyancy Determine the Horizontal Scale of
512 Convective Self-Aggregation. *J. Atmos. Sci.*, **75**, 469–478, https://doi.org/10.1175/jas-d-17-
513 0150.1.

514 Zelinka, M. D., and D. L. Hartmann, 2010: Why is longwave cloud feedback positive? *J.*
515 *Geophys. Res. Atmos.*, https://doi.org/10.1029/2010JD013817.

516 ——, and ——, 2011: The observed sensitivity of high clouds to mean surface temperature
517 anomalies in the tropics. *J. Geophys. Res. Atmos.*, **116**,
518 https://doi.org/10.1029/2011JD016459.

519

520

Supplemental Material for:

Temperatures of Anvil Clouds and Radiative Tropopause in a Wide Array of Cloud-Resolving Simulations

Seth Seidel and Da Yang

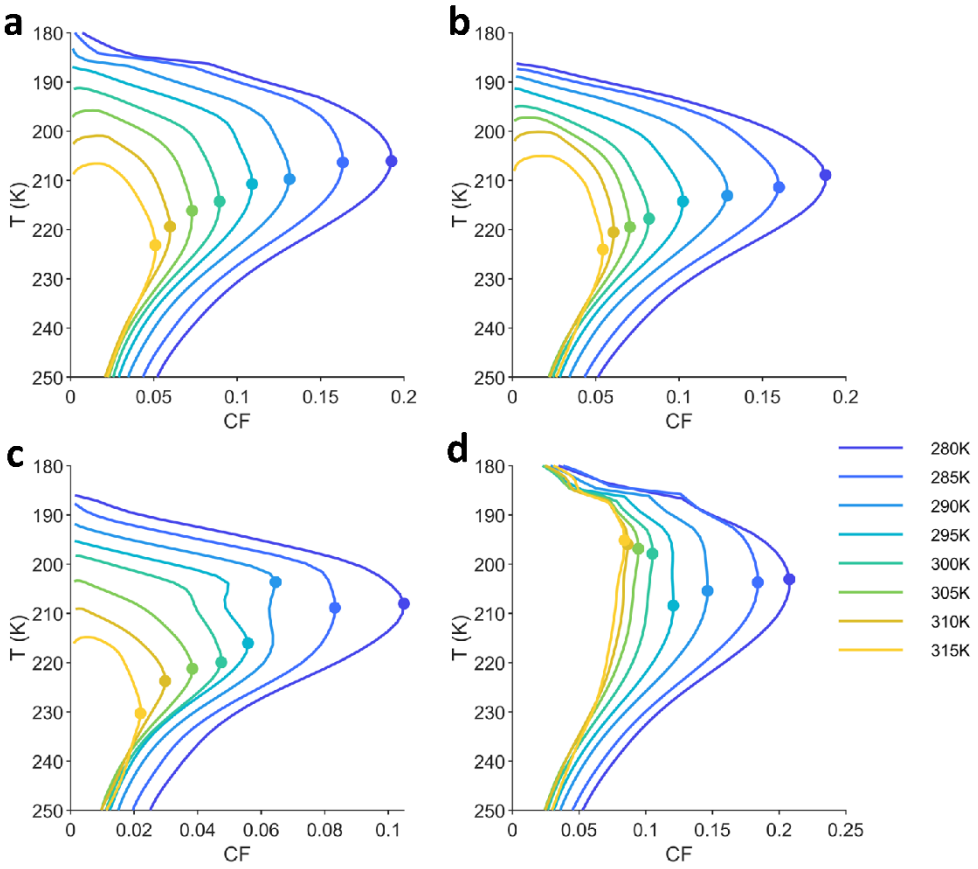

Figure S1. Non-monotonic behavior of the anvil peak. Profiles of cloud fraction, plotted against a temperature coordinate for (a) the Standard experiment, (b) the Standard-no CO_2 experiment, (c) the 2x Solar experiment, and (d) the No O_3 experiment. The circles mark the maximum in upper-tropospheric cloud fraction. In the 2x Solar and No O_3 experiments, temperature of maximum cloud fraction suddenly shifts as the shape of the cloud fraction profile changes.

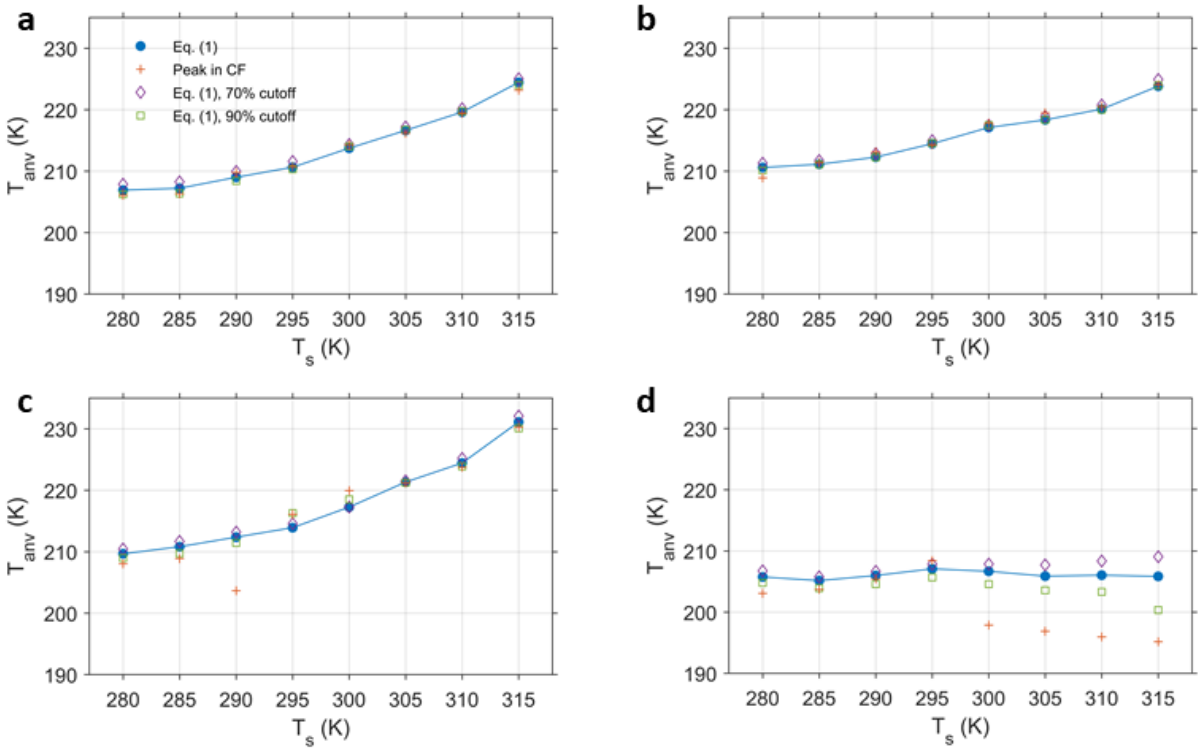

533

534 **Figure S2. Anvil temperature according to several definitions.** To demonstrate the robustness of Eq.
535 (1), we show the anvil temperature as defined by (i) Eq. (1), (ii) the peak in CF (as in Fig. S1), (iii) Eq.
536 (1), modified so that the "anvil" is declined to include all levels where cloud fraction as at least 70% of its
537 maximum value, and (iv) Eq. (1), with a 90% cutoff. The different panels are for (a) the Standard
538 experiment, (b) the Standard-no CO_2 experiment, (c) the 2x Solar experiment, and (d) the No O_3
539 experiment. Note the dependence on definition for the experiment without ozone.

540

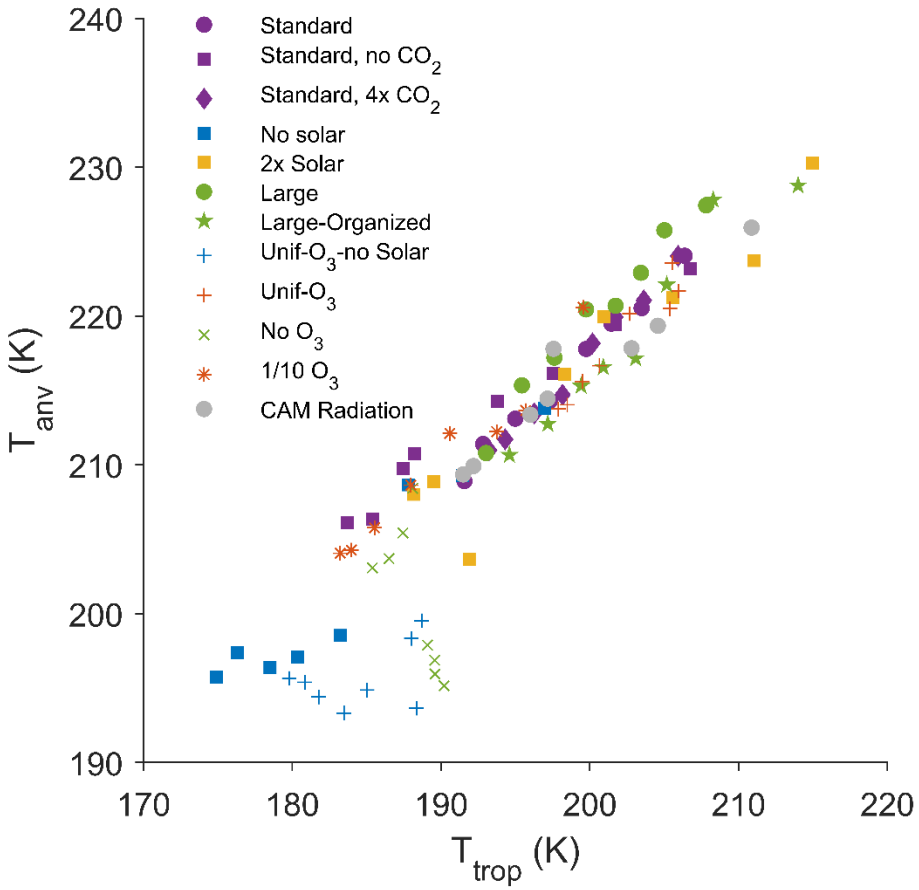

Figure S3. Relationship between T_{trop} and T_{peak}. T_{peak} is the temperature of maximum cloud fraction, as marked in Fig. S1. The tropopause-anvil relationship still holds for most experiments even when the anvil temperature is defined as T_{peak}.